RSC Advances

PAPER

View Article Online
View Journal | View Issue



Cite this: *RSC Adv.*, 2022, **12**, 31943

# Transformation of theranostic alginate-based microbubbles from raspberry-like to core–shell-like microbubbles and *in vitro* studies†

Meng-Yi Bai, *[ab] Tsai-Hsuan Chen,[a] Yu-Chi Wang[c] and Yu-Ju Lai[c]

Received 7th October 2022
Accepted 26th October 2022

DOI: 10.1039/d2ra06298d

rsc.li/rsc-advances

In this study alginate-based microbubbles with a raspberry-like or core–shell-like morphology and with an average particle size of 553.6 ± 69.6 μm were synthesized; this was done through a novel procedure of transforming the structure with a 40 kHz ultrasonication which also stimulated the release of the components inside. Through the use of the electrospray technique in conjunction with agitation processes, components such as shikonin (SHK) and indocyanine green (ICG) were simultaneously encapsulated in alginate microbubbles to produce SHK–ICG alginate microbubbles; these microbubbles had half-maximal inhibitory concentrations of approximately 2.08 and 4.43 μM toward CP70 and SKOV3 ovarian cancer-cell lines, respectively, in an *in vitro* cell model. Moreover, these SHK–ICG alginate microbubbles enhanced brightness by 2.5 fold in ultrasound imaging relative to $CaCl_2$ medium only. In conclusion, SHK–ICG alginate microbubbles have promise for use in theranostics.



## Introduction

Ultrasound sonography is a common medical-imaging technique which does not use ionising radiation. Contrast agents have been employed to expand the scope of sonography applications in medical imaging through the enhancement of backscattering from blood or soft tissues. Typically, the contrast agents are based on microscale bubbles, which are effective for ultrasound wave scattering. Various materials such as albumin, phospholipids, and polymers have been used to construct the shells of the microbubbles (MBs).[1] Additionally, natural polysaccharides, such as alginate (ALG), are now widely used as a shell material for MBs.[2–9] ALG, which is a type of natural polymer composed of sugar monomers, enhances the bioavailability of encapsulated drugs.[10] ALG is also known for its mucoadhesive tendency caused by its anionic nature, which is advantageous for preparing novel drug delivery systems for transmucosal applications. Furthermore, ALG-based materials are crosslinkable, and this property can be achieved by reacting them with divalent ions to cause chelation of the ion by the carboxylate groups of ALG. Owing to this property, the rate of the biodegradability of ALG can be adjusted depending on the desired application. According to the literature review of the present study,[11] current methods—such as those involving microfluidic systems, gas-foaming reactions, and emulsion processes—only allow for the gas-encapsulation type, size, and shell material to be controlled. Although these methods are straightforward to apply,[2–9] they provide only modest improvements. Studies have only reported a decrease in bubble size, a change in the type of encapsulation gas, a modification of the shell material, and the avoidance of the polydispersity of the particles from the use of these methods. Moreover, applications or indications of MBs have now primarily focused on the use of MBs as a contrast agent for ultrasound imaging, particularly for obstetrics and gynaecology.[12] However, obstetricians and gynaecologists may utilise additional imaging technique during ultrasound examinations, such as sentinel lymph node (SLN) mapping. Additionally, obstetricians and gynaecologists can employ theranostics,[12] which is a combination of diagnosis and therapeutics for cancer to reduce metastasis during treatment and prevent recurrence. An enhanced multifunctional and flexible preparation approach is required to produce multimodal MBs that are superior to conventional MBs. We addressed two research gaps here. First, unlike in our previous research,[14] where we synthesised disc-shaped solid microparticles for providing combined therapy to the affected area, in the present study, we completely changed the particle structure from solid to bubble type and reported its potential applications in theranostics. Second, we developed indocyanine green (ICG)-loaded multimodal ALG MBs using the whipping emulsion method with the electrospray (ES)

[a]*Graduate Institute of Biomedical Engineering, National Taiwan University of Science and Technology, No. 43, Keelung Rd, Sec. 4, Da'an Dist., Taipei City 10607, Taiwan. E-mail: mybai@mail.ntust.edu.tw*

[b]*Adjunct Appointment to the Departmnet of Biomedical Engineering, National Defense Medical Centre, Taipei 11490, Taiwan*

[c]*Department of Obstetric and Gynecology, Tri-Service General Hospital, National Defense Medical Centre, Taiwan*

† Electronic supplementary information (ESI) available: A short optical microscopic video showing the fluorescent imaging *in vitro*. See DOI: https://doi.org/10.1039/d2ra06298d

technique to generate raspberry-like MBs. In addition, a simple sonication procedure was used to convert the raspberry-like MBs to core–shell-like MBs; this has not been reported in other studies. These MBs may be used for numerous applications, including encapsulation, targeted drug delivery, controlled release, and as ultrasound contrast agents in medical imaging for theranostics, which demonstrated by the proof-of -concept experiments in this study.

## Experimental

### Materials

ALG was obtained from Sigma-Aldrich (low viscosity, cat. No. A1112-100G; St. Louis, MO, USA). Anhydrous calcium chloride (99%; J. T. Baker, Phillipsburg, NJ, USA), indocyanine green (ICG, 0.25 g, lot-0000028885, Biosynth Carbosynth, Compton, UK), shikonin (SHK; ≥98.0%, 10 mg, PHL89791-10 mg; Sigma-Aldrich), dimethyl sulfoxide (DMSO, ≥99.9%; Sigma-Aldrich), phosphate buffered saline (PBS, 10×, ECHO Chemical, Toufen, Taiwan), and agarose (Sigma-Aldrich) were purchased from the respective manufacturers and used without further purification.

### Preparation of the raspberry-like or core–shell-like SHK–ICG ALG MBs

For the synthesis, 2.9 mg of SHK powder and 10 mg of ICG fluorescent-dye powder were dissolved in 4.08 mL of water–DMSO cosolvent (4 mL of deionised water and 80 μL of DMSO). This mixture was maintained in the dark and frothed with a milk frother for 1–2 min. During the frothing process, 0.15 g of ALG was slowly added to the mixture over 2 min. After all components had completely dissolved in the cosolvent, the resultant solution was withdrawn using a microsyringe, which was equipped with an ES system, per the procedure used in our previous studies.[13] First, the freshly prepared stock solution was supplied using a syringe-pump apparatus (NE-300 Just Infusion; New Era Pump Systems, Farmingdale, NY, USA). A 25-gauge flat-tipped needle was used as the spray needle in the ES procedure. A voltage of +15 kV was applied to the spray needle using a direct-current high-voltage power supply (Bertan Model 205B-20R; Spellman High Voltage Electronics, Hauppauge, NY, USA) to establish an electrical field between the spray needle and the electrically grounded collection solution (10 mL of the 2 wt% $CaCl_2$ aqueous solution maintained under 1000 rpm stirring). The spray needle was placed approximately 4 cm above the surface of the collection solution. The ES modes of the system were monitored by observing the shape of the liquid meniscus at the outlet of the spray needle. Additionally, the meniscus was illuminated with light from an optical cable, and its droplet shape was recorded using a microscopic system comprising a microscopic lens (model: DFK22AUC03, The IMAGING SOURCE, Bremen, Germany), digital camera (model STC-620PWT; Sentech, Carrollton, TX, USA), and high-resolution liquid-crystal display panel. The duration of the ES procedure was 5 min for each run of the MB production. At the end, the obtained MBs floated on top of the collection solution with a green-coloured appearance. For light-microscope characterisation, a 200 μL micropipette was used to draw the top layer of the collection solution, and the sample was transferred onto a glass slide. The specimen was quickly visualised, and the shape of the produced MBs was determined and recorded. The internal composition of the produced MBs was filled with gas, and the shape and internal structure of the MBs were thus easily differentiated under light illumination. The cumulative release of the total encapsulated SHK was determined after triggering by ultrasound supply. The supernatant at each release stage was analysed with spectrophotometry using a SPECTROstar Nano instrument (BMG LABTECH, Ortenberg, Germany).

### *In vitro* cell viability and cytotoxicity studies

A tetrazolium salt 3-[4,5-dimethylthiazol-2-yl]-2,5-diphenyltetrazolium bromide (MTT) assay was performed to assess the viability of the CP70 or SKOV3 cells after treatment with the SHK–ICG ALG MBs. A standard procedure was adopted where the CP70 or SKOV3 cells were seeded in a 48-well plate at a density of $2.5 \times 10^5$ cells per 200 μL (200 μL per well) in DMEM medium for 24 h at 37 °C at a 5% $CO_2$ atmosphere. After 24 h, 200 μL of extract solution of SHK–ICG ALG MBs (SHK–ICG ALG MBs incubated with 10 mL serum-free DMEM medium at 37 °C for 24 h) was added to each well for drug treatment. After another 24 h of incubation at 37 °C in a 5% $CO_2$ atmosphere, the supernatant was removed from each well, and the cells were washed with 500 μL of 1× PBS solution. Finally, 200 μL of MTT reagent was added to each well, and the plate was subsequently incubated for 2 h until purple precipitate was visible. After a predetermined duration, all supernatants were removed and replaced with 200 μL of dimethyl sulfoxide solution. The plate was covered and placed in the dark for 20 min at 37 °C at a 5% $CO_2$ atmosphere. A spectrophotometer was used to measure the optical density of the supernatant at 570 nm. Cell viability was calculated as the ratio of the recorded optical density (OD) values compared to that of the medium only control group according to the following eqn (1):

$$\text{Cell viability} = \text{OD of the drug-treated group} \div \text{OD of the medium only group} \times 100\% \quad (1)$$

### Evaluation of the drug release profile

The real-time drug release profile for the SHK–ICG ALG MBs was determined in a reciprocal shaking water-bath tank that was heated to 37 °C and shaken at a speed of 100 rpm. A typical procedure was adopted where 10 mL of the 2 wt% $CaCl_2$ aqueous solution with dispersed SHK–ICG ALG MBs was maintained in a 20 mL glass-sample vial. At predetermined time intervals, 2 mL of the supernatant was withdrawn, and the dispersion was replenished with 2 mL of the fresh $CaCl_2$ aqueous solution. The supernatants harvested at each release

stage were analysed by spectrophotometry using a SPECTROstar Nano instrument (BMG LABTECH, Ortenberg, Germany).

### Acquisition of ultrasound image

A cylindrical empty pit was moulded in 2% agarose. Generally, 2% agarose is considered a low-backscattering medium. It was used to hold the aqueous suspension of the MBs for acquiring the ultrasound images. Acoustic images were acquired using a high-frequency ultrasound imaging system (GE, Voluson E8, Chicago, IL, USA) with a 9 L high-frequency 2D probe. The *in situ* ultrasound images were stored as digital files for visualising the differences and comparing them with the blank sample (*i.e.*, the agarose mould). All images were mapped to the grayscale values using custom software plugins for ImageJ (W. H. Rasband, NIH, Bethesda, MD, USA).

## Results and discussion

Scheme 1 presents a schematic of the synthetic protocol of the ALG MBs developed in this study (Scheme 1B and C) and its differences from its counterparts in our previous research, which were plate-like solid microparticles (Scheme 1A, the inset image is the scanning electron microscopy image indicating plate morphology and the abundance of production, but the low magnification optical image is unable to reveal these features).[14] The primary difference between the present study and our earlier studies was the facile and easy agitation procedure that was used during the preparation of the ALG-based stock solutions. During agitation, many air bubbles were generated in the viscous stock solution, which was then fed by an ES system, and micrometre-sized droplets were created and sprayed in the air. The $CaCl_2$ aqueous solution was used as the collection substrate, which could crosslink the air bubbles containing ALG *in situ*. The crosslinked droplets finally generated the raspberry-like ALG MBs floating on the top surface of the $CaCl_2$ aqueous solution. These raspberry-like ALG MBs were then converted to core–shell-like ALG MBs or solid spheres upon being passed through an ultrasonic processor (40 kHz, 300 W).

Scheme 2 illustrates the plausible mechanism of raspberry-like SHK–ICG ALG MBs generation. First, SHK and ICG were codissolved in DMSO–water cosolvent because SHK is relatively hydrophobic and only exhibited relatively low solubility in DMSO–water cosolvent approximately 11 mg $mL^{-1}$. However, it was observed that when the SHK–ICG cosolvent mixed with ALG,[15] the viscosity of this ALG-based stock solution increased remarkably and helped to maintain the persistence of air bubbles created by the agitation process before the bubbles were crosslinked by the reported calcium ions. Considering the UV-vis spectra (Fig. S1†), alginate shows a strong absorption peak at 293 nm, which is known to be the n–π* transition absorption of carbonyl group on carboxylate (O=C–$O^-$). However, when the alginate mixed with ICG, the UV-vis absorption spectra show a strong near infrared absorption peaks at 706 nm and 778 nm but the peak related to the alginate carbonyl group (O=C–$O^-$) remarkably red shift to 392 nm. Typically, This red shift of the n–π* transition absorption of carbonyl group indicated the possible interaction with some other functional groups through hydrogen or electrostatic boding, which weaken the bond strength of the carboxylate group. Thus, we proposed that the ionic gelation was formed between alginate polymeric chain and ICG molecules through electrostatic interaction.[16,17] Hence, the most likely encapsulation site of SHK was inside the air bubbles, which was well secured by the described crosslinking procedure. This was in response to the ultrasound-assisted drug release profile in

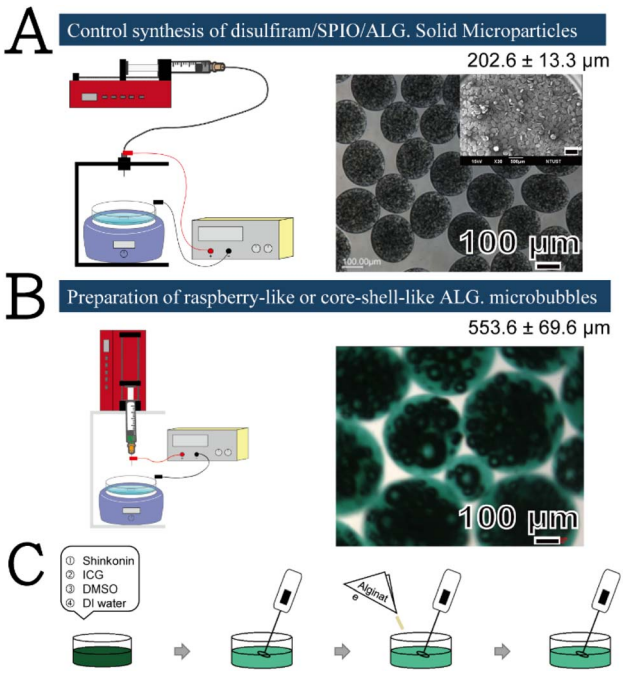


Scheme 1 Schematic illustration of the (A) a comparison to our previous plate-like solid microparticles and (B and C) synthetic protocol of the ALG MBs developed in this work. The scale bar in the inset image in (A) represents 500 μm.

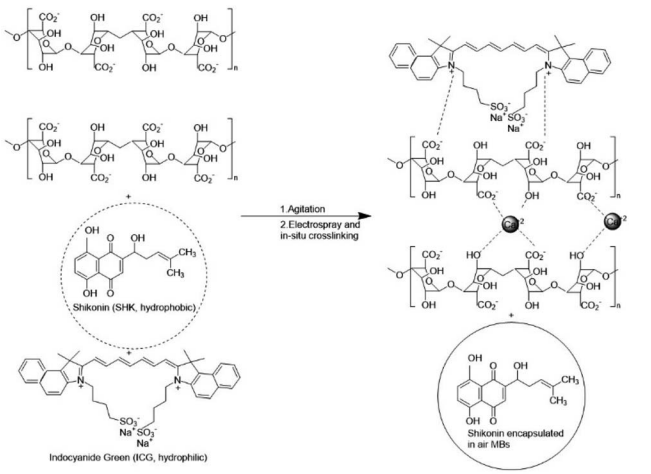


Scheme 2 Schematic illustration of the plausible mechanism of raspberry-like SHK–ICG ALG MBs formation in this work.

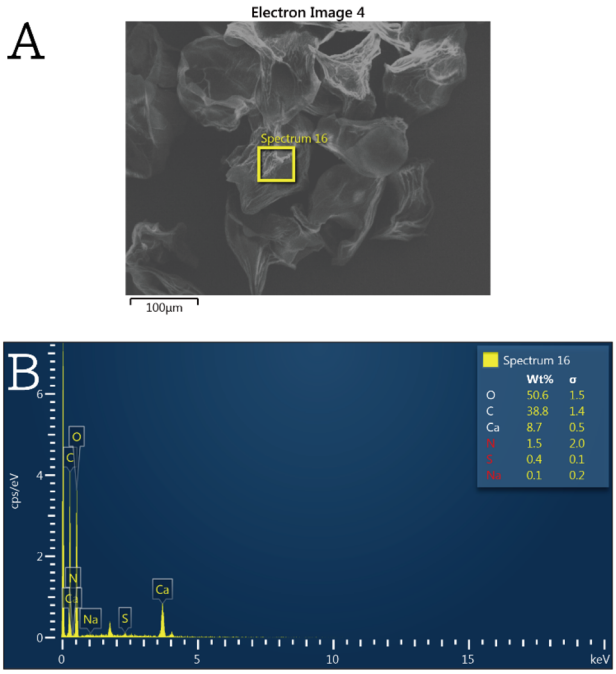


Fig. 1 (A) SEM image of an individual SHK–ICG ALG MB sample after being subject to ultrasonication and freeze–drying and (B) its energy dispersive X-ray (EDX) spectrum.

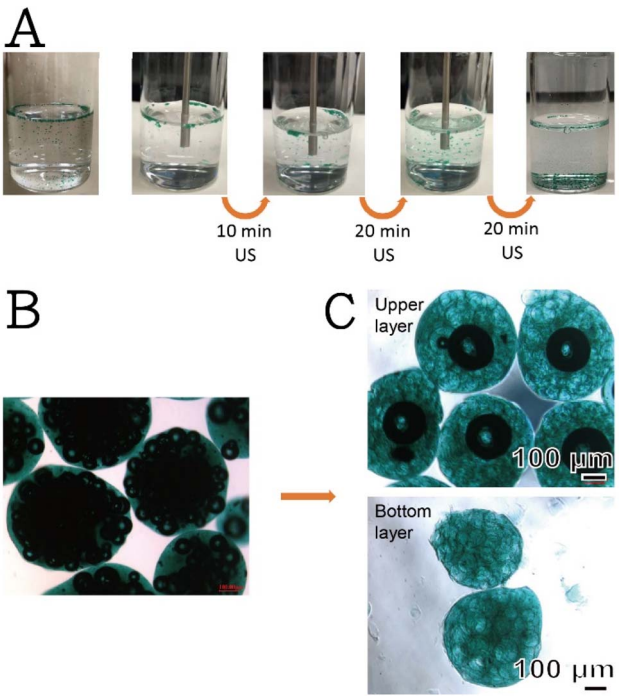


Fig. 2 Optical images show (A) a series of time-dependent images of the freshly generated SHK–ICG ALG MBs after being subject to untrasonication, (B) the morphology of the freshly prepared SHK–ICG ALG MBs, which shows a raspberry-like shape, and (C) two different types of particles harvested after raspberry-like MBs were subject to 50 min untrasonication, *i.e.*, core–shell-like SHK–ICG ALG MBs and solid particles.

Fig. 1A, which indicated 0% SHK release before 5 min ultrasound oscillation.

In order to prove the crosslinking mechanism and the ionic gelation of ICG to ALG proposed in Scheme 2, SEM equipped with an energy dispersive X-ray (EDX) detector was used to characterize SHK–ICG ALG MBs' chemical composition. As can be seen in Fig. 1A, an individual SHK–ICG ALG MBs sample after being subject to ultrasonication and freeze–drying is found to be porous from inward to outward. The selected area EDX spectrum shows the characteristic elements C, O, Ca, N, S, Na, which can be attributed to crosslinking ALG, ICG and SHK. Also, based on the calculated atomic ratio obtained from the EDX spectrum (see Table S1†), the crosslinking degree of the ALG was estimated to be 95.3%, which was according to the plausible mechanism shown in Scheme 2 that each repeating unit of ALG is chelating two calcium ions (theoretical atomic ratio = 3.4%). This high crosslinking degree helps with elucidating the nearly no fluorescent level of ICG detected in the suspension liquid (see ESI† video material), which indicated that the ICG were well encapsulated in the crosslinked ALG shell. On the other hand, the porous channel created from inward to outward after the MBs were being subject to ultrasonication provided the channel for drug encapsulated to diffuse out.

Fig. 2A presents a series of time-dependent images of the freshly generated SHK–ICG ALG MBs prepared under the most optimum condition currently found (see Fig. S2–S4† for results of different parameter trials). Initially, all MBs were floating on top of the water surface, similar to most reported MBs in the literature; however, after ≥10 min of ultrasonication, some particles settled at the bottom of the bottle. Fig. 2B presents the original morphology of the freshly generated SHK–ICG ALG MBs. The particle size was estimated to be 553.6 ± 69.6 µm, and its morphology resembled a raspberry with many small bubbles on the inside. Notably, after these raspberry-like SHK–ICG ALG MBs were subjected to ultrasonication for more than 30 min, many particles settled at the bottom and some were still floating on top of the water surface. After 50 min, these two portions of the samples were taken for optical microscopy characterisation (Fig. 2C). Unexpectedly, the morphology of the originally floating MBs transformed from being raspberry-like to being core–shell-like with a considerably higher bubble volume (4 285 081.9 $\mu m^3$) than that of the original (202 542.6 $\mu m^3$). This may be due to the merging and growth of the inside of the bubble. By contrast, for the settled-down particles (Fig. 2C, bottom layer), all encapsulated air bubbles inside the ALG MBs imploded and empty cavities were left inside. Considering these observations, we investigated why some particles settled instead of floating after being subjected to ultrasonication, which also offered a facile and easy route to produce the core–shell-like SHK–ICG ALG MBs. Based on other researchers' MBs studies, people already understood that the MBs expands during ultrasonication. During expansion, microbubbles may also come into contact with each other, resulting in coalescence or bounce with each other.[18,19] The shell ruptures upon expansion, exposing clean free bubble interfaces that for merge with each other. However, this only occurs only for whose time scales

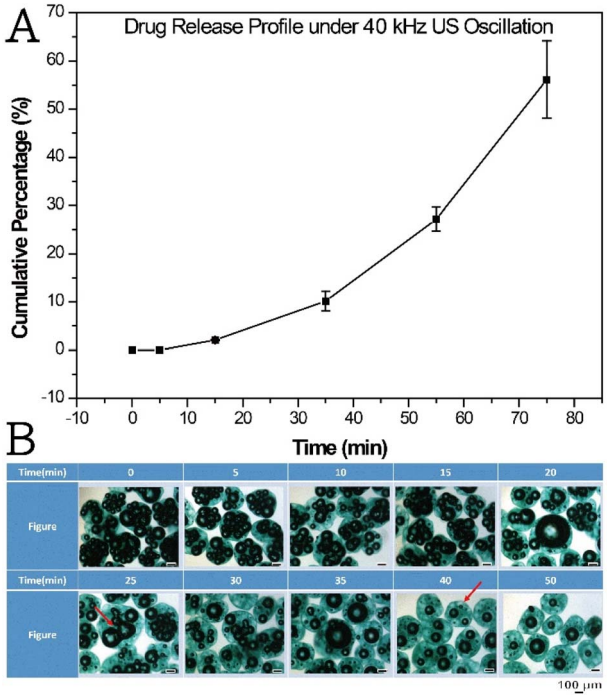


Fig. 3 (A) The drug release profile of SHK–ICG ALG MBs measured at different time points under 40 kHz ultrasonication and (B) the optical images of the MBs sampled at different time points. The scale bar in the inset image represents 100 μm.

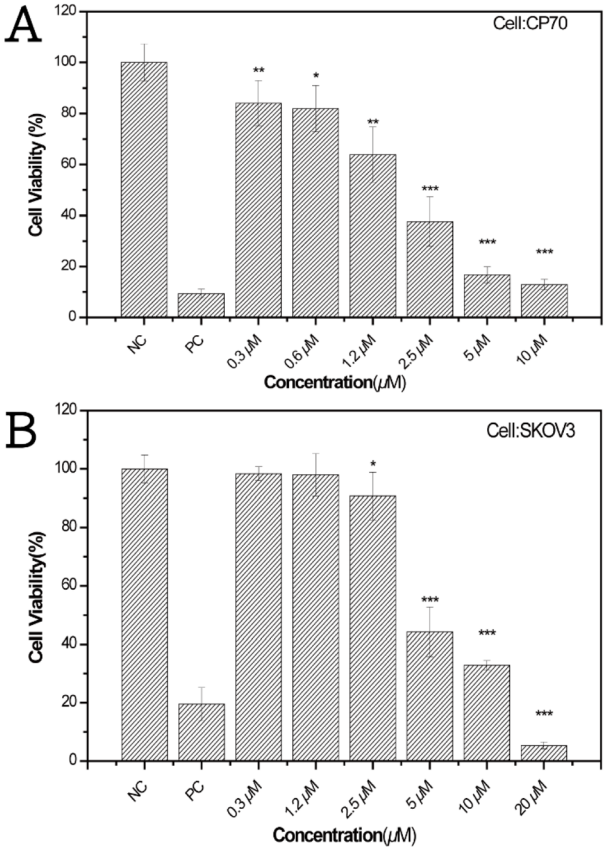


Fig. 4 MTT assays against two human ovarian cancer-cell strains, (A) CP70 and (B) SKOV3 cell strain, both human ovarian cancerous cells were treated with ultrasound-assisted extract solution of SHK/ICG ALG MBs for 24 h. *P*-value < 0.05 was considered to be significant.

match those of the observed coalescence. Researchers have found that small bubbles are more prone to undergo coalescence than larger bubbles because of the smaller drainage timescales involved.[18] Their research is an echo to our studies why the core–shell-like SHK–ICG ALG MBs with a larger bubbles at the centre were remained after ultrasounication. The implosions of the small bubbles inside the MBs prompted us to investigate the possibilities of ultrasound-assisted drug release and imaging bimodalities for their applications in theranostics.

First, the time-dependent drug release profile was monitored (Fig. 3A). Under 40 kHz ultrasonication, the encapsulated SHK drug was released. Notably, the level of the freeform of the SHK drug was close to 0%, which indicated that the drugs were well encapsulated in the crosslinked ALG shell. However, as the duration of ultrasonication increased, the cumulative drug release percentage increased; this was probably caused by the ruptured bubbles inside the ALG shell. The implosion of the bubbles created a pathway for outward diffusion. The MBs sampled during the drug release determination (Fig. 3B) clearly indicated the merging and cavity of the bubbles (indicated by the red arrowheads in Fig. 3B and S5A†). To prove our observation and hypothesis, those particles after being subject to ultrasonication were harvested, freeze–drying and being submitted for optical and SEM acquisition (Fig. S5B and C†). Fig. S5A† shows the optical image of SHK–ICG ALG MBs after being subject to ultrasonication. A clear rupture of the bubble is seen on top of the particle surface. Owing to the occurrence of these two responses inside the SHK–ICG ALG MBs upon ultrasonication, the conversion of raspberry-like to core–shell-like structures simultaneously induced the drug release, but most of the MBs still maintained a coalescence bubble at the centre of their cores.

In addition to the determination of drug release ability, the cytotoxicity of the SHK–ICG ALG MBs against CP70 and SKOV3 cells was evaluated. Fig. 4 presents the cytotoxicity assays against two human ovarian-cancer-cell strains, CP70 and SKOV3, which were treated with ultrasound-assisted extract solution of SHK–ICG ALG MBs for 24 h. The SHK–ICG ALG MBs exhibited a greater cytotoxicity toward CP70 than did the SKOV3 cells. The test concentration was a series of half-dilutions starting from 20 μM, and the IC50 values could be estimated from the spline interpolation of individual cell viability assays (see ESI, Fig. S6 and S7†), which were approximately 2.08 and 4.43 μM for CP70 and SKOV3, respectively. Additionally, the SHK–ICG ALG MBs exhibited dose-dependent cytotoxic activity against both ovarian-cancer-cell lines. Hyun *et al.* reported that SHK mainly acts by inducing apoptotic cell death through the endoplasmic reticulum and mitochondria-mediated pathways to exert cytotoxic effects on the cancerous cells.[20] Therefore, we believe that the released drug acted through a similar mechanism to combat cancer cells, with the exception being that the drug release could be controlled by applying ultrasonication at specific time intervals for activation. The ICG and core bubbles inside the MBs can be used for fluorescent imaging and sound-

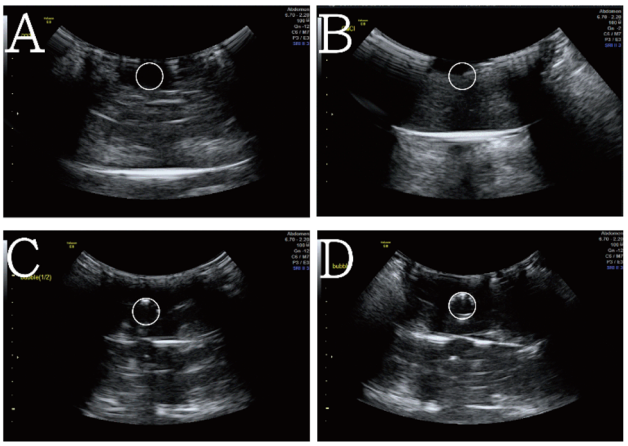


Fig. 5 Ultrasound-scanned images of the (A) blank agarose phantom, (B) $CaCl_2$ aqueous solution with precipitated solid ALG solid particles, (C) 0.5× SHK/ICG ALG MBs suspension and (D) 1× SHK/ICG ALG MBs suspension.

backscattering images of the SLN and enables waves to be reflected off the body structures. A self-made agarose phantom model was constructed (Fig. S8†) to evaluate the improvements in ultrasound imaging provided by the SHK–ICG ALG MBs. In general, the system for ultrasound measurements comprised a diagnostic medical-ultrasound instrument, an agarose phantom with an array of Eppendorf-shaped pits in the centre to hold the SHK–ICG ALG MBs suspension, and control samples.

Fig. 5 presents the ultrasound-scanned images of the blank agarose phantom, $CaCl_2$ aqueous solution with precipitated solid ALG solid particles, 0.5× SHK–ICG ALG MBs suspension, and 1× SHK–ICG ALG MBs suspension. The pure agarose gel is translucent to sound waves, and thus the background of its ultrasound-scanned image was completely dark (Fig. 5A). By contrast, the image for the $CaCl_2$ aqueous solution exhibited a slight background contribution (Fig. 5B, brightness value: 21.9). When the SHK–ICG ALG MBs were loaded, only the central portion corresponding to the MB suspension was bright (Fig. 5C and D, brightness value: 45.1 and 53.8, respectively). In particular, we observed many bright, visible, and white dots at the edge of the phantom hole. These bright spots were generated by the SHK–ICG ALG MBs, in contrast to the control and *in situ* snapshot images before the measurements (see Fig. S8B†). The ultrasound probe emerged from the side wall of the agarose phantom (Fig. S8A†), and once it interacted with the shells of the MBs and caused them to oscillate, the MBs were pushed forward and gathered at the edge of the circle. However, the same phenomenon was not observed in the solid ALG particles, which were collected after being ruptured and settled down at the bottom of the phantom hole (see Fig. S8A,† top-right sample image).

Fig. S9B† and the fluorescent video (see ESI†) present the SHK–ICG ALG MBs injected into a uterine myoma (Fig. S9A†). Notably, the suspension traversed along the lymphatic channel, and MBs carried with green ICG can be clearly observed. When the imaging system was changed from a bright field to a near infrared system, fluorescent emission behaviour was observed. Notably, the fluorescent emission only emitted from where the MBs were located and nonfluorescence was emitted from the phosphate buffer saline suspension liquid. The included images demonstrate that the ICG were well confined in the ALG shell possibly by the ionic gelation interaction as described in Scheme 2. Hence, no freeform of ICG were observed in the suspension liquid, and these MBs are expected to more precisely indicate the SLN in imaging compared with imaging using freeform ICG.

## Conclusions

In summary, we present an easy and facile procedure for synthesising raspberry-like and core–shell-like SHK–ICG ALG MBs using an ES system in combination with agitation and ultrasonication. The agitation of the stock solution played a crucial role in the generation of numerous tiny bubbles in the ALG shells. Subsequently, the ALG solution was electrosprayed and crosslinked for 24 h to encapsulate the small bubbles and drug components inside the shell and bubble simultaneously, thus serving therapeutic and diagnostic functions. Therefore, the drug release and ultrasound imaging enhancement can be initiated from these raspberry-like or core–shell-like SHK–ICG ALG MBs. Because the MBs could be produced with multicore, multicomponent encapsulation and flexible composition, this ES-based method could also be scaled up for the high-volume production of MBs composed of various core and shell material pairs. These MBs may be used for a wide range of applications, including encapsulation, targeted delivery, and controlled release; they can also be used as ultrasound contrast agents in medical imaging.

## Author contributions

M. Y. Bai authored the first draft of the manuscript and prepared all of the figures. M. Y. Bai and T. H. Chen conducted all studies associated with the design of the experiments, setup of the ES system, materials preparation, and cell model assays. Y. C. Wang and M. Y. Bai collaborated to produce the revised version of this manuscript. Y. J. Lai contributed to the studies associated with ultrasound imaging acquisition.

## Conflicts of interest

There are no conflicts to declare.

## Acknowledgements

This work was supported by the grant number MOST 111-2221-E-011-151, Taiwan.

## Notes and references

1 S. Shashank and B. Mark, *Bubble Sci., Eng., Technol.*, 2009, **1**, 3–17.

2 A. Bilal, S. Eleanor and E. Mohan, *Food Bioprocess Technol.*, 2012, **5**, 2848–2857.
3 K. S. Huang, Y. S. Lin, W. R. Chang, Y. L. Wang and C. H. Yang, *Molecules*, 2013, **18**, 9594–9602.
4 Y. Chih-Hui, W.-T. Wang, G. A. Mihai, H. Keng-Shiang and L. Yung-Sheng, *Nanoscale Res. Lett.*, 2014, **9**, 277–285.
5 E. I. Ayisigi, P. S. Metiner, G. Manzi, K. Giannasi, W. V. Hoeve and O. Y. Celiktas, *Macromol. Biosci.*, 2020, **20**, 2000084–2000091.
6 F. Baghbani, F. Moztarzadeha, J. A. Mohandesi, F. Yazdianc and M. M. Dizaji, *Int. J. Biol. Macromol.*, 2016, **93**, 512–519.
7 M. Elsayed, J. Huang and M. Edirisinghe, *Mater. Sci. Eng., C*, 2015, **46**, 132–139.
8 J. Park, E. Tumarkin and E. Kumacheva, *Macromol. Rapid Commun.*, 2010, **31**, 222–227.
9 F. Baghbani, M. Chegeni, F. Moztarzadeh, J. A. Mohandesi and M. M. Dizaji, *Mater. Sci. Eng., C*, 2017, **77**, 698–707.
10 G. A. Martău, M. Mihai and D. C. Vodnar, *Polymers*, 2019, **11**, 1837–1864.
11 H. Lee, H. Kim, H. Han, M. Lee, S. Lee, H. Yoo, J. H. Chang and H. Kim, *Open Biomed. Eng. Lett.*, 2017, **7**, 59–69.
12 J. S. Abramowicz, *Ultrasound Interact. Biol. Med.*, 1997, **23**, 1287–1298.
13 Y. H. Lee, M. Y. Bai and D. R. Chen, *Colloids Surf., B*, 2011, **82**, 104–110.
14 M. Y. Bai, T. T. Wang, S. H. Chen, Y. C. Wang and M. H. Yu, *ChemistrySelect*, 2020, **5**, 7797–7802.
15 K. Nigorikawa, K. Yoshikawa, T. Sasaki, E. Iida, M. Tsukamoto, H. Murakami, T. Maehama, K. Hazeki and O. Hazeki, *Mol. Pharmacol.*, 2006, **70**, 1143–1149.
16 S. S. Lee, H. Kim, D. K. Sohn, J. B. Eom, Y. S. Seo, H. M. Yoon and Y. Choi, *Quant. Imaging Med. Sur.*, 2020, **10**, 779–788.
17 H. Liang, X. Chen, R. Jin, B. Ke, M. Barz, H. Ai and Y. Nie, *Small*, 2020, **16**, 1906538–1906550.
18 M. Postema, P. Marmottant, C. T. Lancée, S. Hilgenfeldt and N. D. Jong, *Ultrasound in Medicine & Biology*, 2004, **30**, 1337–1344.
19 T. Ay, X. Havaux, G. V. Camp, B. Campanelli, G. Gisellu, A. Pasquet, J. F. Denef, J. A. Melin and J. L. J. Vanoverschelde, *Circulation*, 2001, **104**, 461–466.
20 H. Xia, A. K. Kyoung, J. P. Mei, X. Z. Ao, J. H. Yu, M. K. Hyun, S. R. Yea and W. H. Jin, *Biomol. Ther.*, 2019, **27**, 41–47.